Reynolds number dependency in compressible crossflow-jet problems

Guillermo Araya[1]*, Christian J. Lagares-Nieves[1,2†] and Kenneth Jansen[3] ‡

[1]*Computational Turbulence and Visualization Lab., Dept. of Mechanical Eng., University of Texas at San Antonio, TX 78249, USA.*

[2]*Dept. of Mechanical Eng., University of Puerto Rico at Mayaguez, PR 00681, USA.*

[3]*Dept. of Aerospace Eng. Sciences, University of Colorado at Boulder, CO 80309, USA.*

Compressible jets transversely issuing into a spatially-developing turbulent boundary layer (SDTBL) are one of the most challenging types of three-dimensional flows due to their thermal-fluid complexity and technological applications; for instance, film cooling of turbine blades, fuel, or dilution air injection in gas turbine engines, thrust vector control, just to name a few. The ability to control a flow field in such a way as to enhance thermal efficiency is of crucial relevance in aerospace and other engineering applications. We seek to perform Direct Numerical Simulation (DNS) with high spatial and temporal resolution of compressible jets in crossflow at low ($\delta^+ \approx 250$) and high ($\delta^+ \approx 1000$) Reynolds numbers. The analysis will be done by prescribing accurate turbulent flow information (instantaneous velocity, temperature and pressure) at the inlet of the computational domain for simulations of SDTBL based on the Dynamic-Multiscale Approach (DMA) by Araya *et al.* [1], and more recently extended to supersonic/hypersonic flow [2–5]. Extensive DNS cases are planned (sonic jets interacting with subsonic crossflow at $M_\infty = 0.8$). Furthermore, the extensive data supplied by DNS will allow us to elucidate the jet-SDTBL interaction on the complex vortex system (or coherent structures) generated downstream and to gain a better knowledge on the different processes of the vorticity transport (such as stretching, tilting and diffusion). The high spatial/temporal resolution and numerical accuracy of DNS, combined with the objective mathematical framework of the Lagrangian Coherent Structure (LCS) approach, will shed important light on the physics behind the complex set of flow structures in compressible crossflow jets, shock formation, flow separation and jet boundaries.

I. Nomenclature

Re_{δ_2}	=	Momentum thickness Reynolds number
M_∞	=	Freestream Mach number
U_∞	=	Freestream velocity
U^+_{VD}	=	Van Driest transform velocity in wall units
T_∞	=	Freestream temperature
T_r	=	Recovery or adiabatic temperature
T_w	=	Wall temperature
ν_w	=	Wall kinematic viscosity
u_τ	=	Friction velocity
P	=	Mean Static Pressure
T	=	Mean Static Temperature
k	=	Thermal conductivity
c_p	=	Specific heat at constant pressure

*Associate Professor, Department of Mechanical Engineering, University of Texas at San Antonio, San Antonio, TX, 78249. AIAA Associate Fellow, araya@mailaps.org, https://ceid.utsa.edu/garaya/

†PhD Research Assistant & Doctoral Candidate, Department of Mechanical Engineering, 259 Alfonso Valdez Blvd., Mayaguez, PR, 00680, and Student Member, christian.lagares@upr.edu

‡Professor, Dept. of Aerospace Eng. Sciences, University of Colorado at Boulder, CO 80309. AIAA Associate Fellow, kenneth.jansen@colorado.edu

μ = Dynamic Molecular Viscosity
ρ = Fluid Density
δ = Boundary layer thickness
δ^+ = Friction Reynolds number
τ = Shear stress
$_{inl}$ = inlet plane variable
$_{rec}$ = recycle plane variable
$_{rms}$ = Root-Mean Squared
$'$ = Superscript denotes fluctuating components
$^+$ = Superscript denotes inner or wall units
$_\infty$ = Subscript denotes freestream quantities

II. Introduction

In the last few decades, the compressible transverse jet has been extensively analyzed due to its importance in technological applications, including fuel or air injection in gas turbine engines, thrust vector control for high-speed air-breathing and rocket systems [6]. The injected fluid typically has a different velocity and temperature than those of the freestream flow, yielding a flow field (extremely three-dimensional not only instantaneously but also on the time average) with a high level of turbulence and large temperature differences. These turbulent fluctuations have been shown experimentally to affect the downstream properties of the crossflow fluid, Kamotani & Greber [7]. They also concluded that the velocity and temperature distributions principally depended on the momentum flux ratio of the jet to the crossflow. Furthermore, a complicated set of flow structures and vortex systems is generated by the interaction of the jet with the crossflow (Fric & Roshko [8]): the shear-layer vortices, the counter-rotating vortex pair (CVP), the wake vortices and the horseshoe vortex, as seen in figure 1 for transonic crossflow interacting with a supersonic jet, Beresh *et al.* [9].

These vortical or coherent structures have been the motivation of several studies by many researchers: Fric & Roshko [8], Kelso *et al*. [10], Karagozian [11], New *et al*. [12], Muldoon & Acharya [13] and Sau & Mahesh [14]. *In spite of the significant progress performed in the last thirty years, modeling efforts for crossflow jets have been hindered by a lack of information on large-scale structures generated at the jet boundaries, which are responsible for the significant entrainment of fluid*.

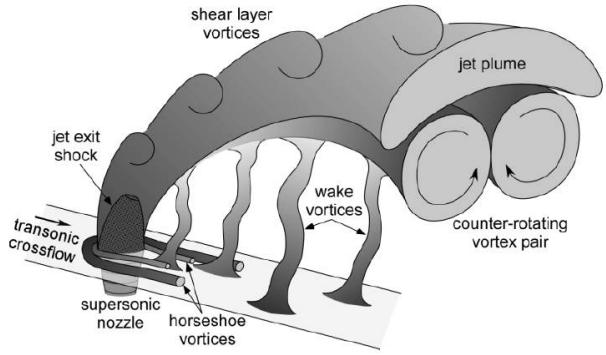

Fig. 1 Vortices in crossflow jet. Adapted from [9]

According to Mahesh [15], a transverse jet at low-velocity ratio shows global instability, high anisotropy, and non-equilibrium characteristics, which represents an enormous challenge for its accurate understanding. Furthermore, the coherent structures emanating from a crossflow jet permit rapid mixing between the jet and crossflow species, a greatly desired feature in staged combustion for both fuel and air injection [16, 17]. It is well known that the dominant vortical structure in the wake of a crossflow jet situation is the counter-rotating vortex pair (CVP) [18]. On the other hand, some technological applications may request minimal flow mixing, for instance, the film-cooling technique [19]. Furthermore, film cooling (a classical example of crossflow jet in aerospace) is widely used in turbomachinery and rocket propulsion applications [20]. Comprehensive summaries on film cooling studies can be found in review articles by [21] and [22]. There is a detrimental effect of the CVP on the film-cooling effectiveness over the downstream wall since it enhances vertical mixing; therefore, significant research effort has been invested in order to assess the effects of different external conditions of the counter-rotating vortices [21]. For instance, Smith and Mungal [23] experimentally studied the trajectory, scaling, and structure of crossflow jets at very high-velocity ratios from extensive imaging of the planar concentration field. A series of experiments were performed at the University of Karlsruhe in crossflow jets by Andreopoulos & Rodi, including flow visualization study and spectral analysis [24], measurement of mean and fluctuating velocity and temperature [25], [26]. Bagheri *et al.* [27] carried out an analysis on the three-dimensional formation and stability of vortices formed during the interactions of jets in crossflow. They concluded by means

of selective frequency damping that high-frequency unstable global eigenmodes were associated with shear-layer instabilities on the CVP, meanwhile, low-frequency modes were linked to shedding vortices in the wake of the jet. Steady and time-periodic blowing/suction flow perturbations in a turbulent boundary layer were prescribed by [28]. They concluded that time-periodic blowing/suction disturbances with a forcing frequency of $f^+ = 0.044$ proved to be more efficient in enhancing local pressure fluctuations and exciting the very small scales in a turbulent channel flow than by steady perturbation.

In terms of high-speed crossflow jets, Santiago and Dutton [29] performed an experimental study of a sonic, underexpanded, transverse, round jet injected into a Mach 1.6 crossflow. They employed laser Doppler velocimetry (LDV) to measure all three mean velocity components as well as five of the six Reynolds stresses. Principal conclusions in [29] are as follows: i) an important recirculation region was observed upstream of the jet, indicating that this region could be used as an ignition zone in combustion, ii) jet plume spreading is crucial in the design of a supersonic combustor, iii) the presence of large Reynolds shear stresses in the shear layer might indicate high level of correlation among turbulent structures, and iv) the stagnation point on the windward side of the barrel shock is characterized by the presence of highly 3D and unsteady events with large velocity gradients. *As for the latter outcome, they also recommended special attention of the mesh size effects and turbulence models in numerical studies*. Beresh and his team [9, 30–32] experimentally investigated the problem of transverse overexpanded supersonic jets issuing into a subsonic compressible turbulent spatially-developing crossflow via Particle Image Velocimetry (PIV) analysis. It was concluded that peak values of the Reynolds stresses increased and moved farther from the wall for larger ratios of the jet-to-freestream dynamic pressure, J, whereas the crossflow Mach number kept almost constant.

Turning our attention to numerical simulations of turbulent wall-bounded flows, DNS is a numerical method for solving the full Navier-Stokes equations without any turbulence model. This is a step up over all other numerical tools since it resolves the physics at the smallest scales of turbulence, i.e. Kolmogorov and Obukhoff-Corrsin scales, for the momentum and thermal field, respectively. Another numerical tool in the Computational Fluid Dynamics (CFD) community is Large Eddie Simulation (LES). It is a compromise of DNS in the sense that instead of resolving all turbulence scales (from the large scale motions to the smallest scales), LES prescribes certain filter functions to the small scales and solve the rest of the scales as done by DNS, [33]. Certainly, the extensive information supplied by DNS demands significant computational resources not only during the running stage but also in the database postprocessing. A number of LES studies were carried out at low Reynolds numbers with the purpose of comparing to Santiago & Dutton's [29] experimental investigation. Rana *et al.* [34] performed implicit LES (iLES) of a sonic transverse jet injection into a supersonic crossflow via a synthetic turbulent inflow data generation. The Reynolds number used in iLES was six times smaller compared to the experiment in [29]; hence, their inlet friction Reynolds number was roughly $\delta^+ \approx 300$. And the initial conditions were based upon the experimental study by Santiago & Dutton [29] as well. Kawai & Lele [35] carried out LES over a similar crossflow jet situation and geometry as in [34] at $\delta^+ \approx 500$, obtaining fair agreement in first order statistics (i.e., time-averaged streamwise and wall normal components of the fluid velocity) when compared with experiments by [29]. Chai *et al.* [36] also performed LES and dynamic mode decomposition (DMD) to scrutinize an underexpanded sonic jet injected into a supersonic crossflow [29] and an overexpanded supersonic jet injected into a subsonic crossflow [30]. They used the compressible dynamic Smagorinsky model, being the Reynolds numbers one-fourth and one-sixth of the experiments, respectively, due to computational cost.
Recent advances in flow simulations with high spatial-temporal resolution (i.e., direct numerical simulations) have opened up the possibility of enhancing the insights behind jets in incompressible crossflow [37], [13] and [38]. The effects of Favorable Pressure Gradient (FPG) and local blowing perturbations (crossflow jet), in isolated or combined forms, were examined in incompressible SDTBL with passive scalar transport via DNS [39, 40]. It was found that the upward motion induced by CVPs encountered the downward flow coming from the inviscid and irrotational outer region, generating a clear shear layer. This layer was characterized by high level of turbulence intensities (secondary peaks), TKE, turbulent mixing and thermal fluctuations. Furthermore, turbulent structures showed an oblong or elongated shape with a spanwise squeezed silhouette due to the stretching process induced by FPG.

In summary, the performed literature review has revealed the scientific importance of turbulent jets in high-speed crossflow. In addition, "quantitative data at high speeds are less common, and visualization still forms an important component in estimating penetration and mixing", as articulated by [15] in his well known review article. Additionally, Santiago and Dutton [29] emphasized "the dearth of quantitative, nonintrusive measurements of the mean velocity and turbulence fields" in transverse jet injection into a supersonic flow. The present study will focus on a fundamental and

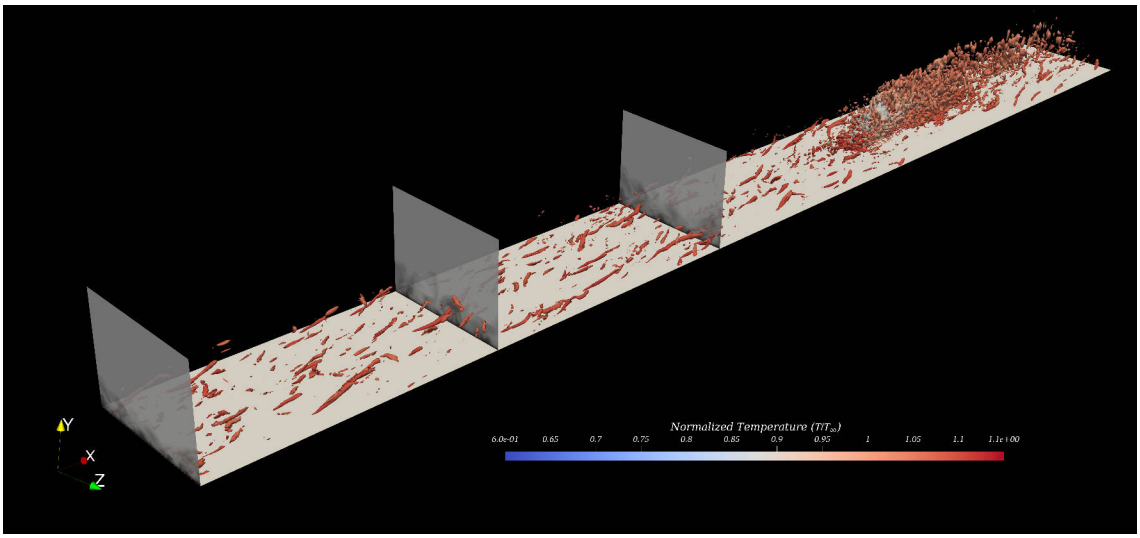

Fig. 2 Schematic of the subsonic spatially-developing boundary layer with Inlet, Recycle and Test planes and sonic jet at low Reynolds numbers (flow from left to right). Iso-surfaces of $Q_{criterion}$ colored by local static temperature.

comprehensive study on the compressible crossflow jet problem at moderately high Reynolds numbers via HPC (both, in the running and postprocessing stages), as well as a particle advection scheme for Lagrangian Coherent Structure (LCS) analysis.

III. Turbulent Inflow Generation and Flow Solver for HPC

One of the crucial aspects on the simulations of unsteady spatially-developing boundary layers (SDTBL) is the prescription of accurate and realistic turbulent inflow information. In the proposed study, we are making use of a type of rescaling-recycling method [1, 41–43], which is an improvement to the original rescaling-recycling method by Lund *et al.* [44]. The seminal idea of the rescaling-recycling method is to extract the flow solution (mean and fluctuating flow components) from a downstream plane (called "recycle") and after performing a transformation by means of scaling functions, the transformed profiles are re-injected at the inlet plane. Since the inlet boundary layer thickness is fixed, the inlet friction velocity is computed based on a power function of the momentum thickness, where the power exponent is "dynamically" calculated "on the fly" according to the flow solution downstream (Test and Recycle planes). Thus, there is no need of an empirical correlation as in other recycling methodologies. More recently, PI's have extended the DMA to compressible spatially-developing turbulent boundary layers (SDTBL) for turbulent inflow conditions [2, 3, 5]. Figure 2 shows the schematic of the computational domain for simulating a crossflow jet under a zero favorable pressure gradient (ZPG) in a subsonic crossflow-sonic vertical jet. A turbulence precursor is attached upstream of the jet. The shown three cross-sectional planes (Inlet, Test and Recycle planes, respectively) with contours of instantaneous streamwise velocity play specific roles in the generation of inflow turbulence, readers are referred to [1] for additional details. An iso-surface of $Q_{criterion}$ was extracted and plotted (colored by static temperature). The typical horseshoe and counter-rotating vortex pair (CVP) structures can be clearly observed over and downstream the sonic jet.

To successfully perform the proposed DNS at high Reynolds numbers, a highly accurate, very efficient, and highly scalable CFD solver is required. PHASTA is an open-source, parallel, hierarchic (2^{nd} to 5^{th} order accurate), adaptive, stabilized (finite-element) transient analysis tool for the solution of compressible [45] or incompressible flows (Jansen [46] and Jansen *et al.* [47]). Combining minimal dissipation numerics and adaptive [48–50] unstructured meshes, PHASTA has been applied to flows ranging from validation on DNS and LES benchmarks such as channel flow and decay of isotropic turbulence [46, 51–53] to cases of practical interest including incompressible ([54, 55] and compressible [3, 50, 56–58] boundary layer flow control and hypersonic flows [2, 5]. As a result PHASTA has a strong track record of supporting closely coordinated experimental-computational studies [50, 54, 56–58]. PHASTA has been shown [47]

to be an effective tool using implicit techniques for bridging a broad range of time and length scales in various flows including turbulent ones (based on URANSS, DDES, LES, DNS). PHASTA has been carefully constructed for parallel performance [55, 59]. PHASTA has also been ported and scaled well on GPU based and XEON-phi based machines. This portable scaling is unprecedented within the CFD community and essential to extending the proposed simulations to relevant Reynolds numbers.

IV. Efficient Particle Advection Scheme for LCS Analysis

It is well known that coherent structures play a vital role on turbulence transport. These structures can be affected based on the conditions imposed on the flow and further can develop in time and space as the flow convects downstream. In this sense, Direct Numerical Simulation (DNS), with millions of "flow and thermal sensors," may shed important light on the unknown aspects of the transport phenomena in compressible crossflow jets and at "non accessible" locations for experiments, for instance in the near wall region or at the microscale level. Generally, these turbulent structures are linked to subjective schemes like thresholding and particular energy content. Due to this, the present Lagrangian approach allows us to identify the important structures in the flow via a rigorous mathematical framework. The use of the Finite-Time Lyapunov Exponent (FTLE) as a means to characterize coherent Lagrangian structures in transient flows was introduced by Haller [60]. FTLE detects separation of all spatial scales in a finite interval of time. The extraction of the FTLE field and its ridges involves first and second order numerical derivatives of the instantaneous velocity. On the other hand, the Finite-Space Lyapunov Exponent (FSLE) detects the time it takes for two particles initially separated by an initial distance of d_o to reach a final value of d_f.

The Lyapunov exponent is a fundamental metric in chaos theory and dynamical systems, quantifying the rate of separation or convergence of infinitesimally close trajectories. It plays a pivotal role in understanding the sensitivity of a system to initial conditions and its inherent chaotic nature. For a dynamical system described by $\dot{x} = f(x,t)$, where $x \in \mathbb{R}^n$ represents the state vector and f is a smooth vector field, the Lyapunov exponent λ can be mathematically defined as:

$$\lambda = \lim_{t\to\infty} \frac{1}{t} \ln \frac{\|\delta x(t)\|}{\|\delta x(0)\|},$$

where $\delta x(t)$ is the deviation of the trajectory from its initial path at time t. This definition captures the exponential rate at which nearby trajectories diverge or converge, providing insights into the stability and predictability of the system. A positive Lyapunov exponent is indicative of chaos, signifying that even small differences in initial conditions can lead to vastly different outcomes over time [61].

The Finite Time Lyapunov Exponent (FTLE) is a variant of the traditional Lyapunov exponent, tailored to capture chaotic behavior over finite time intervals. This makes it particularly valuable for analyzing transient dynamics in fluid flows, where understanding the evolution of fluid elements over time is crucial. The FTLE is defined for a time interval $[t_0, t]$ as:

$$\sigma^t_{t_0}(x_0) = \frac{1}{|t - t_0|} \ln \sqrt{\lambda_{\max}(\Delta^t_{t_0}(x_0))},$$

where $\lambda_{\max}$ represents the maximum eigenvalue of the Cauchy-Green strain tensor $\Delta^t_{t_0}(x_0)$. The Cauchy-Green strain tensor, given by:

$$\Delta^t_{t_0}(x_0) = \left[\nabla\phi^t_{t_0}(x_0)\right]^T \nabla\phi^t_{t_0}(x_0),$$

is a key measure in continuum mechanics, describing the deformation of a material element in the flow. Here, $\phi^t_{t_0}(x_0)$ is the flow map that tracks the evolution of a particle's position from x_0 at time t_0 to its position at a later time t[62, 63].

On the other hand, the Finite Size Lyapunov Exponent (FSLE) extends the concept to finite-sized disturbances, enabling the analysis of spatially extended systems and capturing the dynamics at various scales. FSLE is particularly useful in understanding how disturbances of a certain size evolve over time in a fluid flow. It is defined as:

$$\lambda_\delta(\vec{x}, t_0, \Delta) = \frac{1}{\tau(\vec{x}, t_0, \delta, \Delta)} \ln \frac{\Delta}{\delta},$$

where δ and Δ are predefined thresholds representing the initial and final separations of trajectories, respectively, and $\tau(\vec{x}, t_0, \delta, \Delta)$ is the time required for the separation between two trajectories, initially δ apart, to reach Δ[64, 65].

This measure is instrumental in identifying regions of flow that are sensitive to the scale of perturbations, providing a more comprehensive understanding of fluid dynamics at different scales. In the present project, an efficient and highly scalable GPU particle advection and Lyapunov exponent calculator (Aquila-LCS) has been developed [66].

A. Proposed DNS Cases and Boundary Conditions

Table 1 summarizes the characteristics of the two numerical (2) cases of crossflow jets for low (Case 1) and high (Case 2) Reynolds numbers, as seen in figure 2, i.e. sonic jet-subsonic crossflow types. Here, subscript ∞ stands for freestream or crossflow conditions, whereas subscripts j refers to jet conditions. Information regarding the computational domain dimensions in terms of the inlet boundary layer thickness δ_{inl} (where L_x, L_y and L_z represent the stream-wise, wall-normal and spanwise domain length, respectively) and the mesh resolution in wall units (Δx^+, Δy^+_{min}, Δz^+) is also supplied based on the inlet friction velocity. Case 1 at low Re is composed by a mesh (hexahedrals) with a grid point distribution of 440×60×80, while the point distribution is 990×250×210 in Case 2 at higher Reynolds numbers.

Table 1 Numerical Cases

Case	Re_{δ_2} Range	J	M_∞	M_j	$L_x \times L_y \times L_z$	Δx^+,Δy^+_{min}/Δy^+_{max},Δz^+
1	309-570	1.72	0.8	1	$42.8\delta_{inl} \times 3.3\delta_{inl} \times 4\delta_{inl}$	14, 0.18/13.4, 7.8
2	2066-2468	1.72	0.8	1	$15.1\delta_{inl} \times 3\delta_{inl} \times 3\delta_{inl}$	11.9, 0.2/11, 11

Boundary Conditions: While this study has a major effort on the inflow turbulent boundary conditions, it is important to point out that the top and outflow of the computational domain also presents some challenges. These challenges were resolved in the past by appending a segment beyond the region of study where sponge boundary conditions smoothly dampen the turbulent structures before they reach the boundary which prevents reflections. The lateral boundary conditions are handled via periodicity. No-slip and adiabatic boundary conditions are prescribed on the walls of the flat plate and the nozzle. The working fluid is calorically perfect non-reacting air. At the top surface, the normal component of the velocity is prescribed a zero value (streamline) and freestream values for density and temperature. The jet is modeled by imposing a wall-normal velocity at the surface, in a circle with a radius R. In the present investigation, the orifice diameter, D is approximately 1.3 times larger than the inlet boundary layer thickness, i.e. $\delta_{inl}/D \approx 0.775$, as in [29]. The momentum flux ratio, J, is defined as the ratio between $\rho_j * U_j^2$ to the incoming freestream kinetic energy, $\rho_\infty * U_\infty^2$. We are considering a low momentum flux ratio of 1.72 in both cases, as [29]. A turbulent jet is set, based on the DNS study in turbulent pipes by [67] at $Re_D = 5300$. Figure 3 shows a laminar (parabolic) and turbulent distribution (as assumed in present simulations) of the prescribed vertical velocity at the jet location where r is the distance to the jet center and V_{max} is the surface velocity at the jet center.

V. Numerical Results at Low and High Reynolds Numbers

Inflow turbulent profiles were assessed (upstream of the sonic jet). The most relevant DNS results at low and high Reynolds numbers (Cases 1 and 2) are shown. Fig. 4 (a) depicts the time-averaged streamwise velocity profiles in wall units for present DNS. The Van Driest transform is applied to the subsonic crossflow ($M_\infty = 0.8$), which enables absorption of compressibility effects; and, therefore direct comparison with other DNS incompressible cases. In addition, external incompressible DNS profiles are included ([68] [69] [70] [71]). Overall, a satisfactory collapse is seen among incompressible and subsonic cases. Because of the low Reynolds numbers considered, the log region seems pretty short, or at a steeper slope. Turbulence intensities and Reynolds shear stresses are depicted by fig. 4 (b) in wall units. The present DNS results contrast quite well with those of [69] at very similar Reynolds numbers, except in u'^+ peaks with discrepancies in the order of 5%. In subsonic quantities, the Morkovin scaling is implemented to account for wall-normal density variation, and the profile affinity is encouraging.

In a similar way, the mean streamwise velocity, turbulence intensities and Reynolds shear stresses (i.e., $< u'v' >$) are depicted by fig. 5 in wall units and at higher Reynolds numbers. In fig. 5 (a), profiles of U^+_{VD} and U^+ vs. y^+ are plotted for present DNS at $M_\infty = 0.8$ as well as DNS data from [72] and [68] at the incompressible flow regime but similar Reynolds numbers (where subscript $_{VD}$ stands for Van Driest transform). Generally speaking, the agreement of the present subsonic DNS profile with other DNS results is quite good, meaning that the Van Driest can accommodate

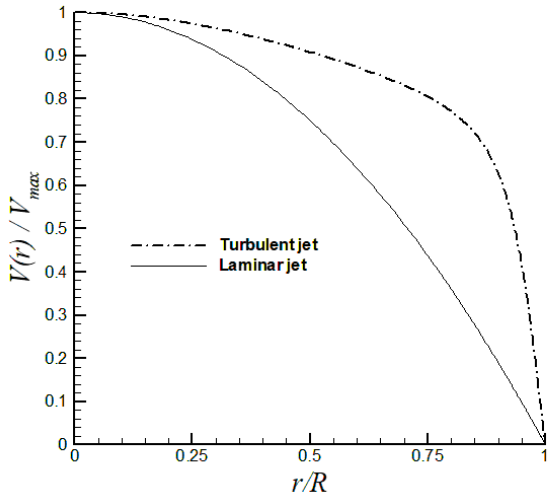

Fig. 3 Wall-normal velocity distribution prescribed at jet location.

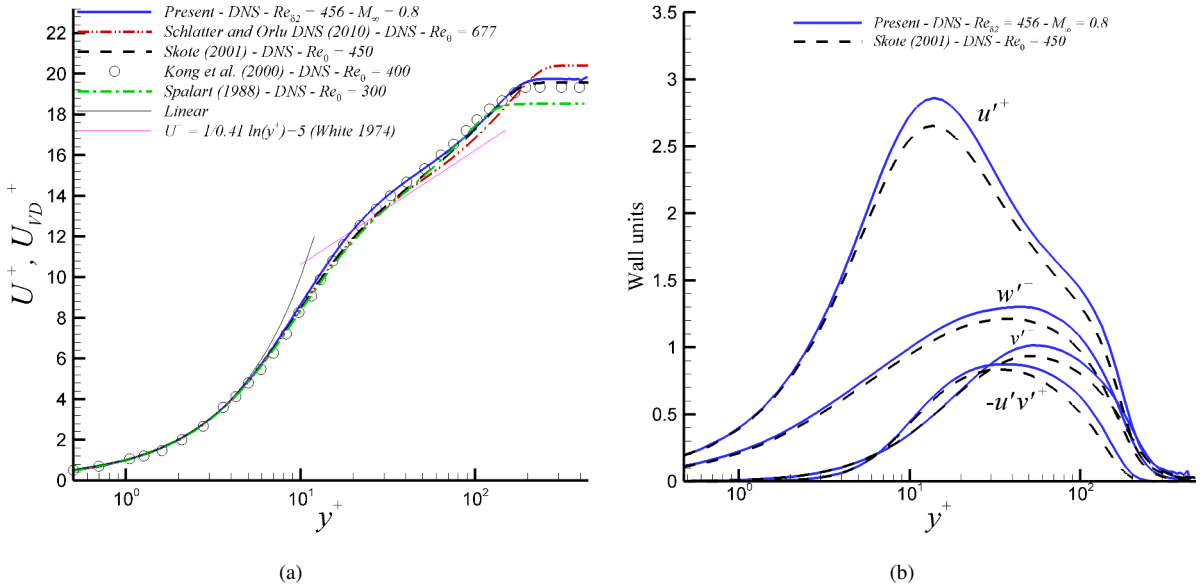

(a) (b)

Fig. 4 Inflow turbulent condition assessment at low Reynolds numbers (Case 1): (a) mean streamwise velocity and (b) turbulent intensities and Reynolds shear stresses.

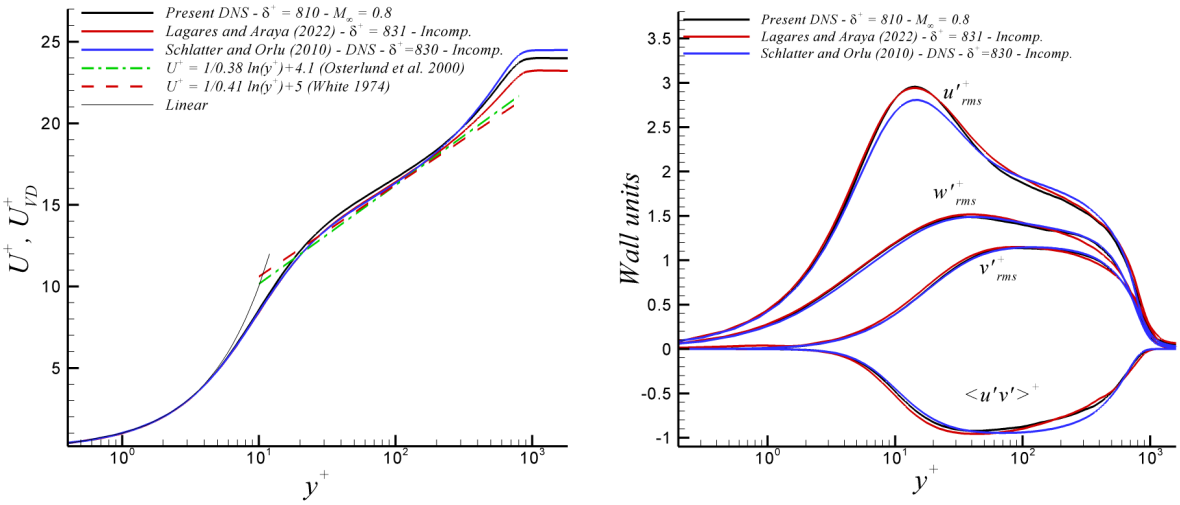

(a) (b)

Fig. 5 Inflow turbulent condition assessment at high Reynolds numbers (Case 2): (a) mean streamwise velocity and (b) turbulent intensities and Reynolds shear stresses.

density variation due to Mach number effects very efficiently. It can be seen some differences in the wake region that can be attributed to small differences in the friction velocity computation. The major Reynolds number effect regarding profiles in fig. 4 (a) is clearly the significant extension of the log region ($20 < y^+ < 200$ or approximately 180 wall units). The proposed log law functions by [73] and [74] describe properly the mean streamwise velocity in the above-mentioned region. Similar outcomes were reported by [3] for an adiabatic Mach-2.5 turbulent flat-plate boundary layer. Furthermore, turbulent intensities (u'^+_{rms}, v'^+_{rms}, and w'^+_{rms}) and the Reynolds shear stresses, $< u'v' >^+$, exhibit a good collapsing level among subsonic ($M_\infty = 0.8$) and incompressible DNS datasets. When contrasting low and high Reynolds number profiles at Mach 0.8 from Fig. 4 (b) and Fig. 5 (b) the following conclusions can be stated: (i) peaks of u'^+_{rms} approximately occur at the same intensity ($\approx$ 2.9-3) and similar wall-normal location ($y^+ \approx 15$), (ii) the constant shear layer extends longer ($30 < y^+ < 300$) at higher Reynolds numbers.

Turning to the mean static temperature in a compressible flow, the T/T_∞ and U/U_∞ relationship is expressed in terms of the Walz's equation,

$$\frac{T}{T_\infty} = \frac{T_w}{T_\infty} + \frac{T_r - T_w}{T_\infty}\left(\frac{U}{U_\infty}\right) - r\frac{\gamma - 1}{2}M_\infty^2\left(\frac{U}{U_\infty}\right)^2 \tag{1}$$

where r is the recovery factor ($= Pr^{1/3}$) and T_r the well known recovery temperature. Figure 6 (b) shows the mean static temperature vs. mean streamwise velocity both normalized by the corresponding freestream value at low and high Reynolds numbers for the incoming ZPG subsonic flow. Overall, the Walz equation gives excellent predictions for the adiabatic subsonic flat plates at low Reynolds numbers. Some discrepancies can be seen at higher Reynolds numbers, particularly around 14% of the boundary layer thickness. However, the error was estimated to be barely 0.56% in terms of the predicted static temperature.

We have also analyzed the skewness and flatness of streamwise velocity fluctuations u'. These third and fourth statistical moments, respectively, serve as measures of the asymmetry and peakedness of the u' distribution [75]. A zero-skewness value indicates a symmetric or Gaussian distribution. Figure 7 (a) shows skewness of u', S_u, at low and high Reynolds numbers of subsonic cases. The very good agreement with incompressible DNS results by [68] at similar high Reynolds numbers reveals the existence of weak compressibility effects. Clearly, the non-zero skewness values in the near wall region ($y^+ < 10$) emphasize the asymmetry of the streamwise velocity fluctuation distribution, potentially demonstrating the existence of dominant one-sided fluctuations, u', in that part of the boundary layer. Since the turbulent flow becomes more isotropic towards the log region, values of S_u close to zero make complete sense within $20 < y^+ < 200$, particularly

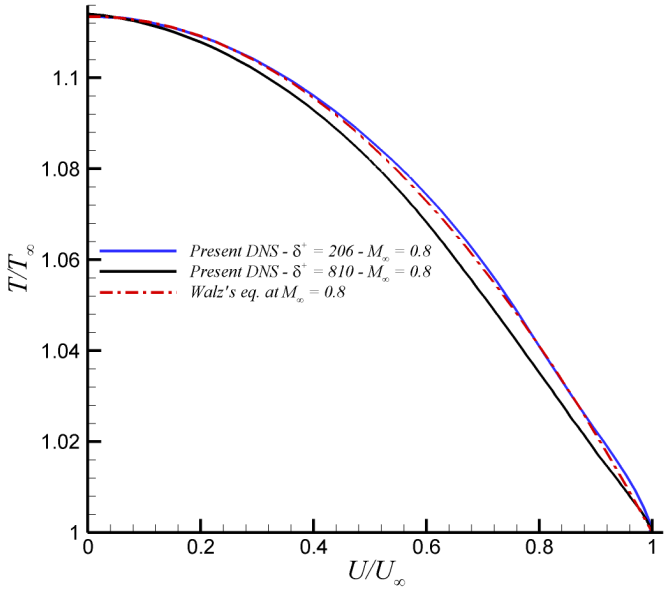

Fig. 6 Mean static temperature at low and high Reynolds numbers (Case 1 and 2).

at high Reynolds numbers. Interestingly, there is a high level of similarity up to $y^+ = 10$ for low and high Reynolds number flows. On the contrary, flatness evidences the presence of extreme and high-amplitude turbulent events. For a Gaussian distribution, the flatness is equal to 3. In figure 7 (b), the flatness of streamwise velocity fluctuations, F_u, is exhibited. Again, the overlap of present DNS at $\delta^+ = 810$ and $M_\infty = 0.8$ with incompressible DNS results by [68] reinforces the presence of weak compressibility effects. In addition, flatness values near 3 in the zone $20 < y^+ < 200$ demonstrate that u' follows a Gaussian distribution. As in the skewness distribution of u', F_u profiles show a strong analogy up to $y^+ = 10$ at the different Reynolds numbers considered, depicting larger values than 3 (≈ 5). Large flatness values in turbulent boundary layers indicate the occurrence of intense and sporadic events, which are a manifestation of intermittency, an inherent property of turbulence.

The skin friction coefficient of the low Reynolds number case is shown by Fig.8 at the centerline plane over the jet center. The streamwise coordinate, x, is normalized by the jet diameter, d. Approximately 3,000 flow fields were gathered for statistics analysis; however, more snapshots might be needed since only time-averaging is performed (not in the spanwise direction). As expected, C_f remains approximately constant upstream of the sonic jet. By a distance of $x/d = -6$ the incoming subsonic flow decelerates due to the presence of a strong adverse pressure gradient. A clear upstream recirculation zone can be observed from $x/d = -1.5$; however, the back recirculation zone is longer, enlarging up to three jet diameters downstream of the sonic flow perturbations.

Three-dimensional (3D) Lagrangian Coherent Structures (LCS) analysis over Case 1 was performed to compare FTLE vs. FSLE attracting material lines by backward integration of particle trajectories in the jet startup. As shown by figure 9, both types of attracting material lines have demonstrated similar flow information by reproducing faithfully jet boundaries and flow recirculating zones (high shear zones). Furthermore, the contours of repelling material lines (forward integration) are depicted by fig. 10 at the centerline plane and based on FTLE and FSLE exponents. In general, both Lyapunov exponents exhibit a similar trend, indicating the presence of highly separated flow zones upstream and downstream of the sonic jet. Figure 11 depicts attracting FTLE contours at cross-sectional YZ planes at the jet center and at two jet diameters downstream of the jet. The presence of a shear layer due to the incoming flow with the vertical jet is clearly observed. In addition, the counter-rotating vortex pair or CVP (mushroom-like structure) can be seen in Fig. 11 (b).

Figure 12 depicts 3D Lagrangian Coherent Structures (LCS) of Case 2 at high Reynolds numbers. In particular, the contours of FTLE and FSLE values by backward integration (i.e., attracting material lines) can be seen in the jet startup based on tracking 416 million particles in the full domain. The provided information by FTLE's and FSLE's about jet

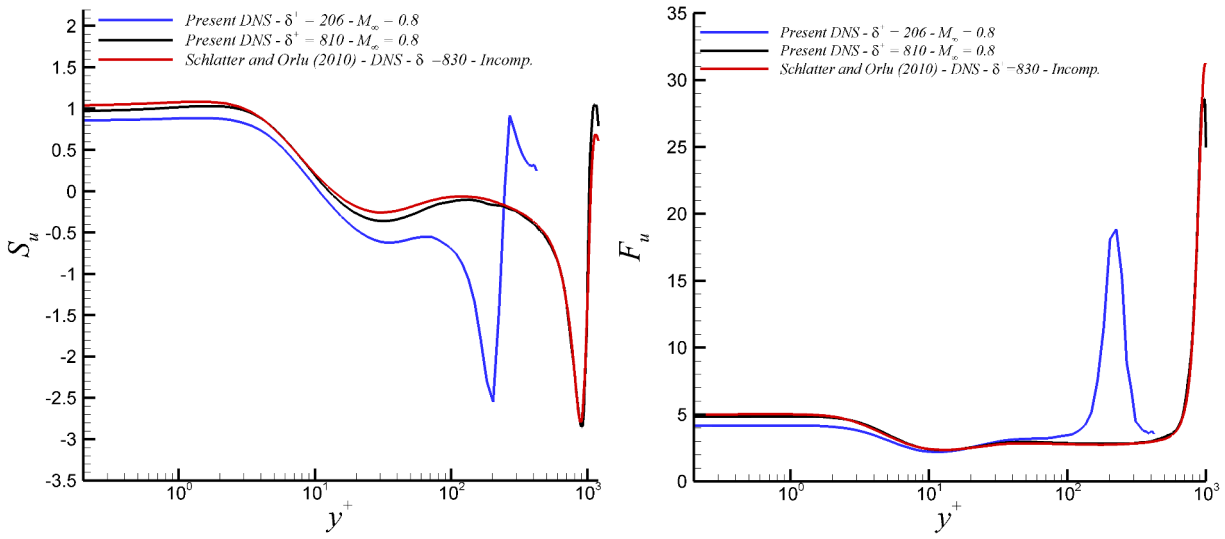

(a) (b)

Fig. 7 Reynolds number dependency in inflow turbulent conditions: (a) skewness of u' and (b) flatness of u'.

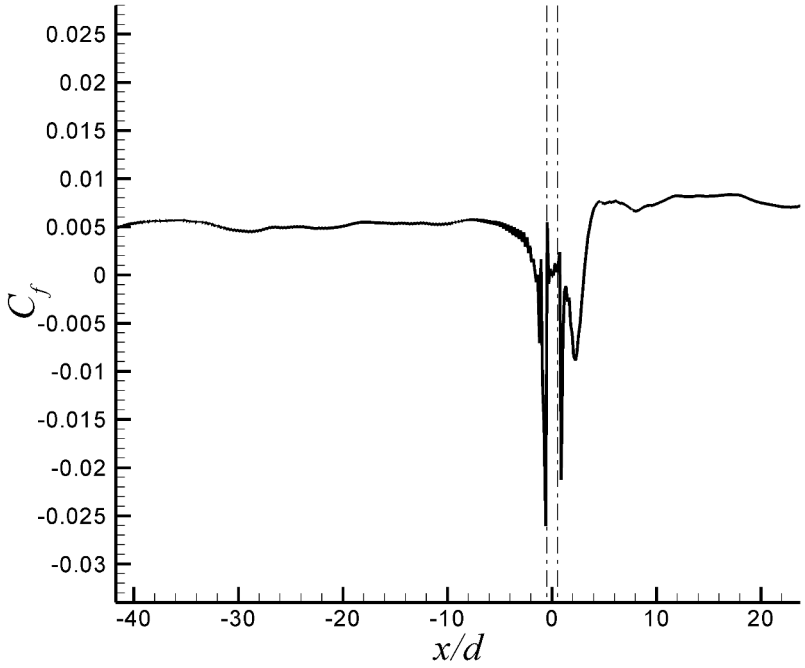

Fig. 8 Centerline skin friction coefficient at low Reynolds numbers (Case 1).

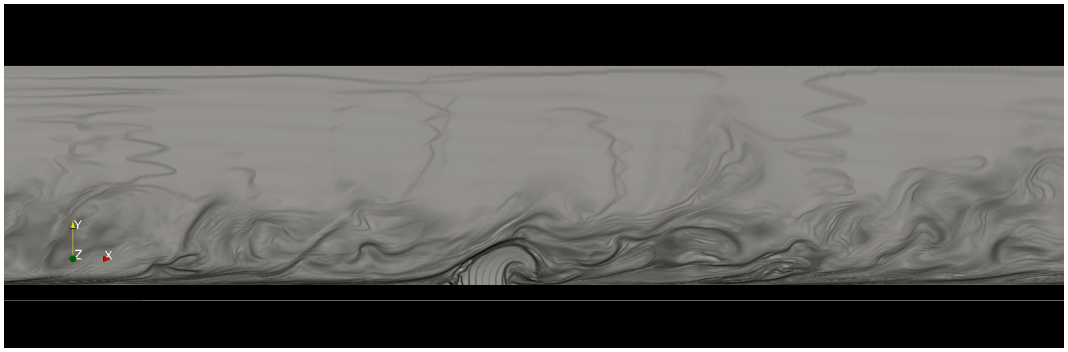

(a)

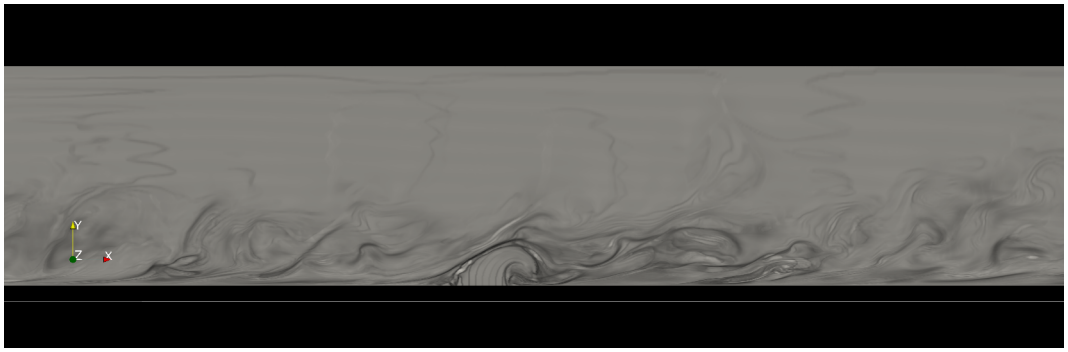

(b)

Fig. 9 Contours of attracting material lines in the sonic jet startup process at low Reynolds numbers: (a) FTLE and (b) FSLE.

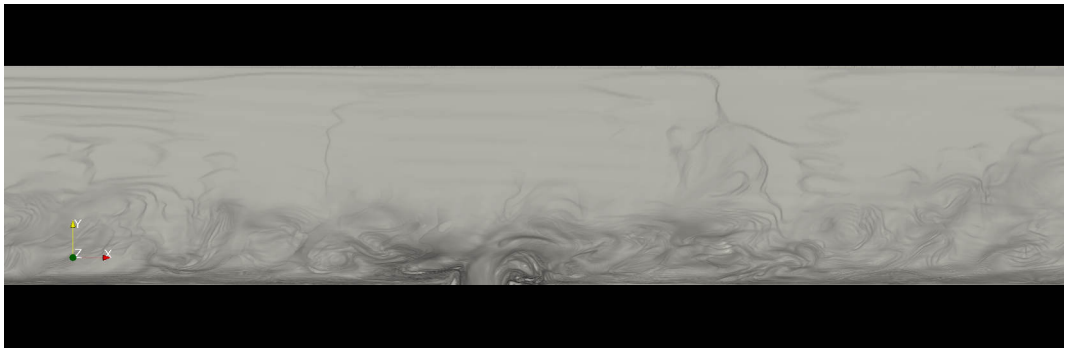

(a)

(b)

Fig. 10 Contours of repelling material lines in the sonic jet startup process at low Reynolds numbers: (a) FTLE and (b) FSLE.

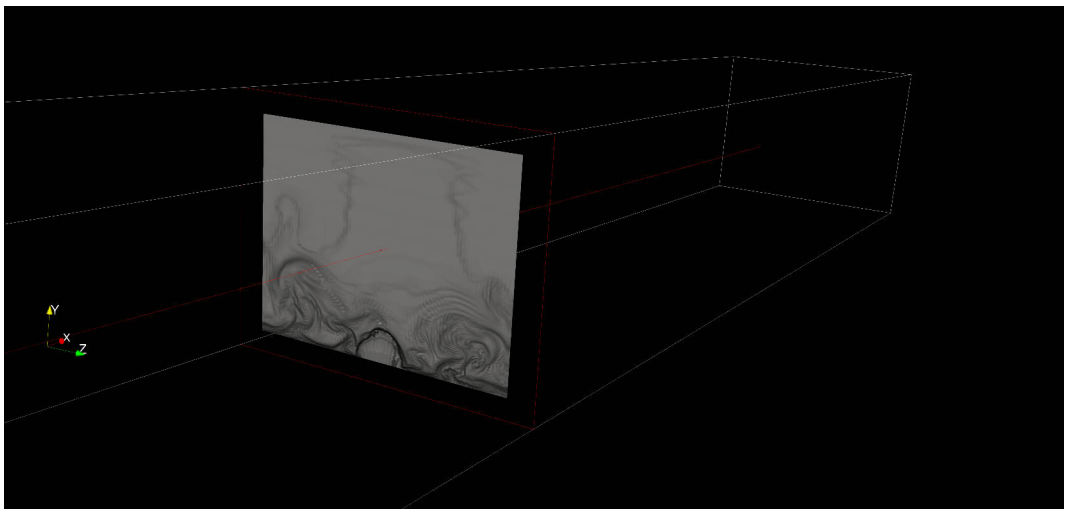

(a)

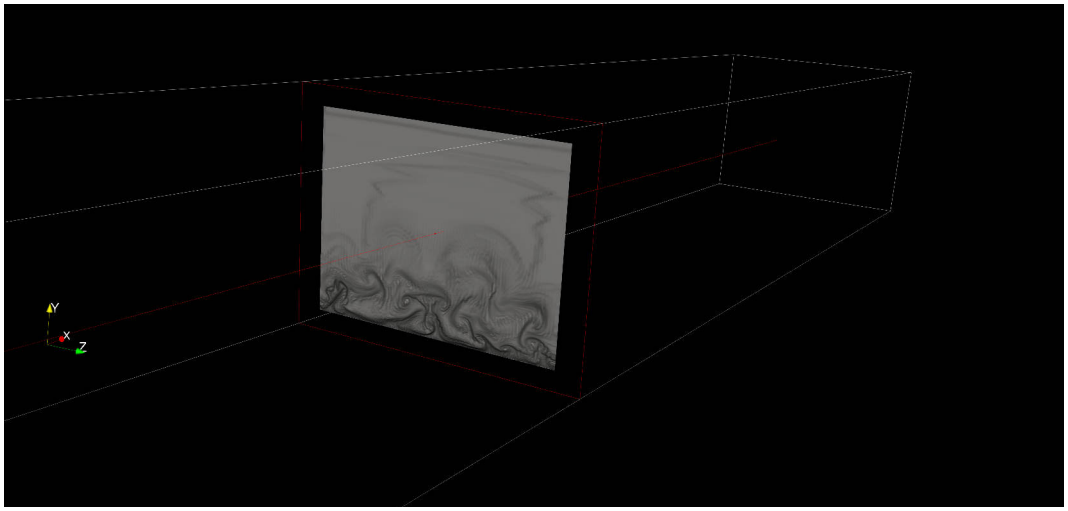

(b)

Fig. 11 Contours of attracting material lines in the sonic jet startup process at low Reynolds numbers: (a) at jet center and (b) 2D from jet center.

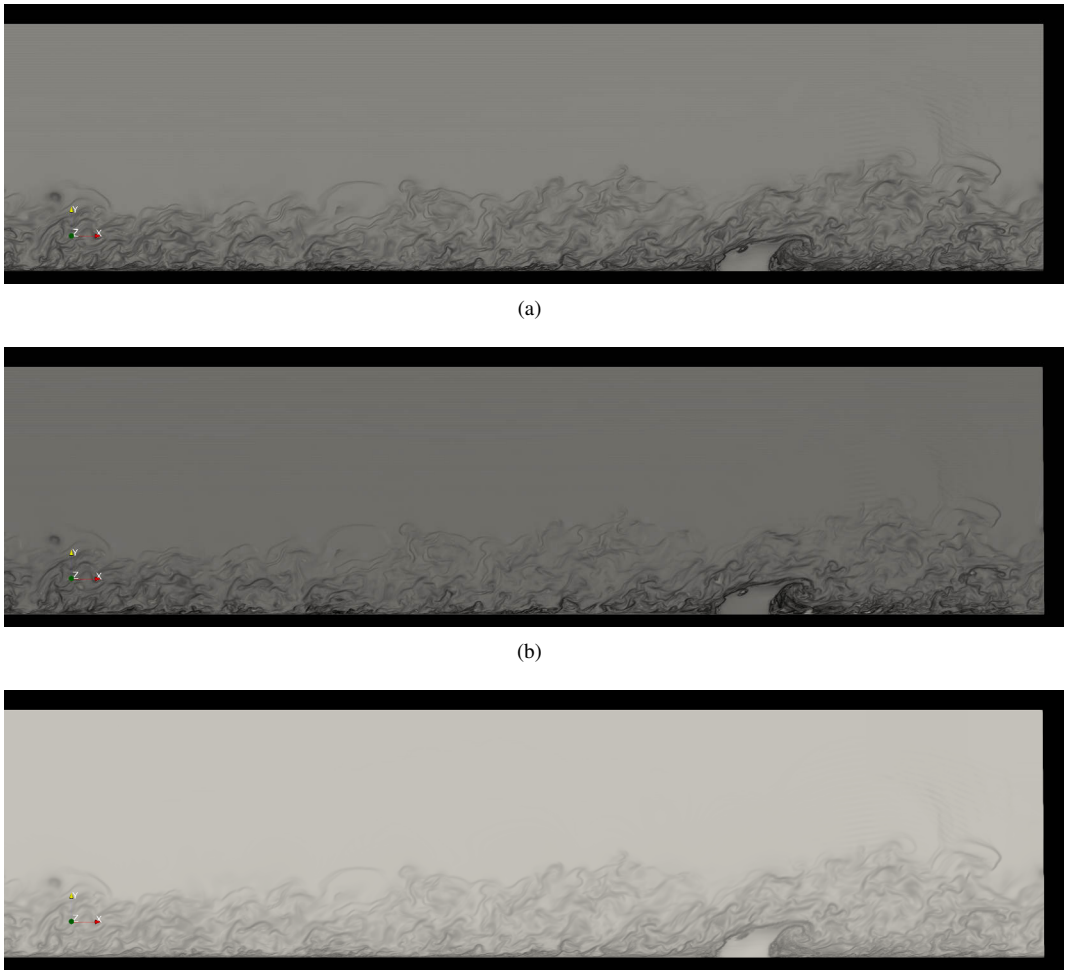

(a)

(b)

(c)

Fig. 12 Contours of attracting material lines in the sonic jet startup process at high Reynolds numbers: (a) FTLE with 416M particles, (b) FSLE with 416M particles, and (c) FTLE with 52M particles .

boundaries, flow recirculating zones, and high shear zones are very similar, as in the low Reynolds number case. In terms of Reynolds number dependency, attracting material lines are more isotropic at higher Reynolds numbers, resembling highly packed and finer structures (less organized and smaller coherent structures). The side views of attracting FTLE ridges describe inclined quasi-streamwise vortices (or hairpin legs) and heads of the spanwise vortex tube located in the outer region. Furthermore, the contours of FTLE in Fig. 12 (c) were obtained by seeding and tracking approximately 52 million particles instead; thus, eight times fewer seeded particles than that in Fig. 12 (a). Generally speaking, one can conclude that the more particles seeded, the more details can be detected in attracting/repelling lines. Furthermore, the global features of inclined quasi-streamwise vortices and hairpin packets [76] are still noticeable for the lower number of particles considered. Also, repelling manifolds by forward temporal integration have been computed and visualized via FTLE and FSLE contours, as seen in Fig. 13. Those manifolds are mostly present in the near-wall region; however, repelling barriers are still observed in the buffer/log region, intersecting hairpin legs in regions where ejections typically occur. Again, the exhibited patterns by FTLE and FSLE look highly analogous at high Reynolds numbers, as well.

(a)

(b)

Fig. 13 Contours of repelling material lines in the sonic jet startup process at high Reynolds numbers: (a) FTLE with 416M particles, (b) FSLE with 416M particles.

VI. Conclusion

In the present study, we are performing Direct Numerical Simulation (DNS) with high spatial and temporal resolution of compressible jets in crossflow at low ($\delta^+ \approx 250$) and high ($\delta^+ \approx 1000$) Reynolds numbers. The incoming turbulence conditions have been validated for both cases. The fulfillment of an acoustic CFL much lower than 1 makes the DNS timesteps very small (in the order of 10^{-4} in terms of Δt^+). Ongoing flow samples are being collected for future low/high order statistics computation in the presence of perturbing sonic jets, including the challenging high Reynolds number Case 2, which is ongoing for sample collection. The LCS analysis performed in the startup process has revealed that attracting material lines better represent jet boundaries and trajectories, with the same level of information from FTLE and FSLE exponents. Future numerical DNS initiatives will involve validation based on experimental studies of [29].

Acknowledgments

This material is based upon work supported by the National Science Foundation under grant #2314303. This material is based on research sponsored by the Air Force Research. Laboratory, under agreement number FA9550-23-1-0241. This work was supported in part by a grant from the DoD High-Performance Computing Modernization Program (HPCMP).

References

[1] Araya, G., Castillo, L., Meneveau, C., and Jansen, K., " A dynamic multi-scale approach for turbulent inflow boundary conditions in spatially evolving flows," *Journal of Fluid Mechanics*, Vol. 670, 2011, pp. 518–605.

[2] Araya, G., Lagares, C., and Jansen, K., "Direct simulation of a Mach-5 turbulent spatially-developing boundary layer," *49^{th} AIAA Fluid Dynamics Conference, AIAA AVIATION Forum, (AIAA-2019-3340) 17 - 21 June, Dallas, TX*, 2019.

[3] Araya, G., Lagares, C., and Jansen, K., "Reynolds number dependency in supersonic spatially-developing turbulent boundary layers," *2020 AIAA SciTech Forum (AIAA-2020-0574) 6 - 10 January, Orlando, FL.*, 2020.

[4] Araya, G., and Jansen, K., "Effects of wall curvature on hypersonic turbulent spatially-developing boundary layers," *2020 AFOSR/ONR/HVSI Hypersonic Aerodynamics Portfolios Review. DOI: 10.13140/RG.2.2.27763.66081*, 2020. https://doi.org/10.13140/RG.2.2.27763.66081.

[5] Araya, G., Lagares, C., Santiago, J., and Jansen, K., "Wall temperature effect on hypersonic turbulent boundary layers via DNS," *AIAA Scitech 2021 Forum (AIAA-2021-1745)*, 2021. https://doi.org/10.2514/6.2021-1745.

[6] Karagozian, A. R., "Transverse jets and their control," *Progress in Energy and Combustion Science*, Vol. 36, 2010, pp. 531–553.

[7] Kamotani, Y., and Greber, I., "Experiments on a turbulent jet in a cross flow," *AIAA Journal*, Vol. 20:11, 1972, pp. 1425–1429.

[8] Fric, T., and Roshko, A., "Vortical structure in the wake of a transverse jet," *Journal of Fluid Mechanics*, Vol. 279, 1994, pp. 1–47.

[9] Beresh, S. J., Henfling, J. F., Erven, R. J., and Spillers, R. W., "Turbulent Characteristics of a Transverse Supersonic Jet in a Subsonic Compressible Crossflow," *AIAA Journal*, Vol. 43, No. 11, 2005, pp. 2385–2394. https://doi.org/10.2514/1.14575.

[10] Kelso, R., Lim, T., and A.E., P., "An experimental study of round jets in cross-flow," *Journal of Fluid Mechanics*, Vol. 306, 1996, pp. 111–144.

[11] Karagozian, A., "The jet in crossflow," *Physics of Fluids*, Vol. 26, No. 101303, 2014, pp. 1–17.

[12] New, T., Lim, T., and Luo, S., "Elliptic jets in cross-flow," *Journal of Fluid Mechanics*, Vol. 494, 2003, pp. 119–140.

[13] Muldoon, F., and Acharya, S., "Direct numerical simulation of pulsed jets in crossflow," *Comput. Fluids*, Vol. 39, 2010, pp. 1745–1773.

[14] Sau, R., and Mahesh, K., "Optimization of pulsed jets in crossflow," *Journal of Fluid Mechanics*, Vol. 653, 2010, pp. 365–390.

[15] Mahesh, K., "The interaction of jets with crossflow," *Annu. Rev. Fluid Mech.*, Vol. 45, 2013, pp. 379–407.

[16] Karagozian, A. R., "Transverse jets and their control," *Progress in Energy and Combustion Science*, Vol. 36, No. 5, 2010, pp. 531–553. https://doi.org/https://doi.org/10.1016/j.pecs.2010.01.001, URL https://www.sciencedirect.com/science/article/pii/S036012851000002X.

[17] Nair, V., Sirignano, M., Emerson, B., Halls, B., Jiang, N., Felver, J., Roy, S., Gord, J., and Lieuwen, T., "Counter rotating vortex pair structure in a reacting jet in crossflow," *Proceedings of the Combustion Institute*, Vol. 37, No. 2, 2019, pp. 1489–1496. https://doi.org/https://doi.org/10.1016/j.proci.2018.06.059, URL https://www.sciencedirect.com/science/article/pii/S1540748918302426.

[18] Fric, T., and Roshko, A., "Structure in the Near Field of the Transverse Jet," *In: Durst F., Launder B.E., Reynolds W.C., Schmidt F.W., Whitelaw J.H. (eds) Turbulent Shear Flows 7. Springer, Berlin, Heidelberg.*, 1991, pp. 225–237. https://doi.org/https://doi.org/10.1007/978-3-642-76087-7_17.

[19] Bogard, D. G., and Thole, K. A., "Gas Turbine Film Cooling," *Journal of Propulsion and Power*, Vol. 22, No. 2, 2006, pp. 249–270. https://doi.org/10.2514/1.18034.

[20] Wernet, M., Wroblewski, A., and Locke, R., "A dual-plane PIV study of turbulent heat transfer flows," *NASA/TM-219074*, 2016.

[21] Goldstein, R. J., "Film Cooling," Elsevier, 1971, pp. 321–379. https://doi.org/https://doi.org/10.1016/S0065-2717(08)70020-0, URL https://www.sciencedirect.com/science/article/pii/S0065271708700200.

[22] Bunker, R. S., "A Review of Shaped Hole Turbine Film-Cooling Technology," *Journal of Heat Transfer*, Vol. 127, No. 4, 2005, p. 441. https://doi.org/10.1115/1.1860562, URL http://heattransfer.asmedigitalcollection.asme.org/article.aspx?articleid=1447794.

[23] Smith, S. H., and Mungal, M. G., "Mixing, structure and scaling of the jet in crossflow," *Journal of Fluid Mechanics*, Vol. 357, 1998, pp. 83–122.

[24] Andreopoulos, J., "On the structure of jets in a crossflow," *Journal of Fluid Mechanics*, Vol. 157, 1985, pp. 163–197.

[25] Andreopoulos, J., and Rodi, W., "Experimental investigation of jets in a crossflow," *Journal of Fluid Mechanics*, Vol. 138, 1984, pp. 93–127.

[26] Andreopoulos, J., "Heat transfer measurements in a heated jet-pipe flow issuing into a cold cross stream," *Physics of Fluids*, Vol. 26, 1983, pp. 3201–3210.

[27] Bagheri, S., Schlatter, P., Schmid, J., P., and Henningson, D. S., "Global stability of a jet in crossflow," *Journal of Fluid Mechanics*, Vol. 624, 2009, pp. 33–44.

[28] Araya, G., Leonardi, S., and Castillo, L., "Steady and time-periodic blowing/suction perturbations in a turbulent channel flow," *Physica D: Nonlinear Phenomena*, Vol. 240, No. 1, 2011, pp. 59–77.

[29] Santiago, J. G., and Dutton, J. C., "Velocity measurements of a jet injected into a supersonic crossflow," *Journal of Propulsion and Power*, Vol. 13, No. 2, 1997, pp. 264–273.

[30] Beresh, S. J., Henfling, J. F., Erven, R. J., and Spillers, R. W., "Penetration of a Transverse Supersonic Jet into a Subsonic Compressible Crossflow," *AIAA Journal*, Vol. 43, No. 2, 2005, pp. 379–389. https://doi.org/10.2514/1.9919.

[31] Beresh, S. J., Henfling, J. F., and Erven, R. J., "Flow Separation Inside a Supersonic Nozzle Exhausting into a Subsonic Compressible Crossflow," *Journal of Propulsion and Power*, Vol. 19, No. 4, 2003, pp. 655–662. https://doi.org/10.2514/2.6154.

[32] Beresh, S. J., Wagner, J. L., Henfling, J. F., Spillers, R. W., and Pruett, B. O. M., "Turbulent eddies in a compressible jet in crossflow measured using pulse-burst particle image velocimetry," *Physics of Fluids*, Vol. 28, No. 2, 2016, p. 025102. https://doi.org/10.1063/1.4940677.

[33] Pope, S. B., *Turbulent Flows*, Cambridge University Press, 2000.

[34] Rana, Z. A., Thornber, B., and Drikakis, D., "Transverse jet injection into a supersonic turbulent cross-flow," *Physics of Fluids*, Vol. 23, No. 4, 2011, p. 046103. https://doi.org/10.1063/1.3570692.

[35] Kawai, S., and Lele, S. K., "Large-Eddy Simulation of Jet Mixing in Supersonic Crossflows," *AIAA Journal*, Vol. 48, No. 9, 2010, pp. 2063–2083. https://doi.org/10.2514/1.J050282.

[36] Chai, X., Iyer, P. S., and Mahesh, K., "Numerical study of high speed jets in crossflow," *Journal of Fluid Mechanics*, Vol. 785, 2015, p. 152–188. https://doi.org/10.1017/jfm.2015.612.

[37] Muppidi, S., and Mahesh, K., "Direct numerical simulation of passive scalar transport in transverse jets," *Journal of Fluid Mechanics*, Vol. 598, 2008, pp. 335–360.

[38] Liu, C., Araya, G., and Leonardi, S., "The role of vorticity in the turbulent/thermal transport of a channel flow with local blowing," *Computers & Fluids*, 2017, pp. 1–17.

[39] Quinones, C., Araya, G., and Chen, Y., "Thermal transport in a crossflow jet subject to a very strong favorable pressure gradient," *Procs. of ASME, IMECE 2017, Nov. 3-9, 2017, Tampa, USA*, 2017.

[40] Quinones, C., "Transport Phenomena in Crossflow Jets Subject to Very Strong Favorable Pressure Gradient," *MSc Thesis, University of Puerto Rico-Mayaguez*, 2020.

[41] G. Araya and L. Castillo, "DNS of turbulent thermal boundary layers subjected to adverse pressure gradients," *Physics of Fluids*, 2013, p. 095107.

[42] Cardillo, J., Chen, Y., Araya, G., Newman, J., Jansen, K., and Castillo, L., "DNS of a turbulent boundary layer with surface roughness," *Journal of Fluid Mechanics*, Vol. 729, 2013, pp. 603–637.

[43] Doosttalab, A., Araya, G., Newman, J., Adrian, R., Jansen, K., and Castillo, L., "Effect of small roughness elements on thermal statistics of a turbulent boundary layer at moderate Reynolds number," *Journal of Fluid Mechanics*, Vol. 787, 2015, pp. 84–115.

[44] Lund, T., Wu, X., and Squires, K., "Generation of turbulent inflow data for spatially-developing boundary layer simulations," *Journal of Computational Physics*, Vol. 140, No. 2, 1998, pp. 233–258.

[45] Whiting, C. H., Jansen, K. E., and Dey, S., "Hierarchical basis in stabilized finite element methods for compressible flows," *Comp. Meth. Appl. Mech. Engng.*, Vol. 192, No. 47-48, 2003, pp. 5167–5185.

[46] Jansen, K. E., "A stabilized finite element method for computing turbulence," *Comp. Meth. Appl. Mech. Engng.*, Vol. 174, 1999, pp. 299–317.

[47] Jansen, K. E., Whiting, C. H., and Hulbert, G. M., "A generalized-α method for integrating the filtered Navier-Stokes equations with a stabilized finite element method," *Comp. Meth. Appl. Mech. Engng.*, Vol. 190, 1999, pp. 305–319.

[48] Zhou, M., Sahni, O., Shephard, M., Devine, K., and Jansen, K., "Controlling unstructured mesh partitions for massively parallel simulations," *SIAM J. Sci. Comp.*, Vol. 32, No. 6, 2010, pp. 3201–3227.

[49] Sahni, O., Luo, X., Jansen, K., and Shephard, M., "Curved boundary layer meshing for adaptive viscous flow simulation," *Finite Elements in Analysis and Design*, Vol. 46, No. 47-48, 2020, pp. 132–139.

[50] Chitale, K., Sahni, O., Shephard, M., Tendulkar, S., and Jansen, K., "Anisotropic Adaptation for Transonic Flows with Turbulent Boundary Layers," *AIAA Journal*, Vol. 53, 2015, pp. 367–378.

[51] Trofima, T.-M. A. J. K., AV, and Lahey Jr, R., "Direct numerical simulation of turbulent channel flows using a stabilized finite element method," *Computers and Fluids*, Vol. 38, 2009, pp. 924–938.

[52] Tejada-Martinez, A., and Jansen, K., "On the interaction between dynamic model dissipation and numerical dissipation due to streamline upwind/Petrov-Galerkin stabilization," *Computer Methods in Applied Mechanics and Engineering*, Vol. 194, 2005, pp. 1225 – 1248.

[53] Tejada-Martinez, A., and Jansen, K., "A dynamic Smagorinsky model with dynamic determination of the filter width ratio," *Physics of Fluids*, Vol. 16, No. 7, 2004, pp. 2514–2528.

[54] Sahni, O., Wood, J., Jansen, K., and Amitay, M., "Three-dimensional Interactions between a Finite-Span Synthetic Jet and a Cross Flow," *Journal of Fluid Mechanics*, Vol. 671, 2011, pp. 254–287.

[55] Rasquin, M., Smith, C., Chitale, K., Seol, S., Matthews, B., Martin, J., Sahni, O., Loy, R., Shephard, M., and Jansen, K., "Scalable fully implicit flow solver for realistic wings with flow control," *Computing in Science and Engineering*, Vol. 21, 2009, pp. 133–154.

[56] Vaccaro, J., Vasile, J., Olles, J., Sahni, O., Jansen, K., and Amitay, M., "Active Control of Inlet Ducts," *Int. J. of Flow Control*, Vol. 21, 2009, pp. 133–154.

[57] Vaccaro, J., Elimelech, Y., Chen, Y., Sahni, O., Jansen, K., and Amitay, M., "Experimental and Numerical Investigation on the flow field within a Compact Inlet Duct," *International Journal of Heat and Fluid Flow*, Vol. 44, 2014, pp. 478–488.

[58] Vaccaro, J., Elimelech, Y., Chen, Y., Sahni, O., Jansen, K., and Amitay, M., "Experimental and Numerical Investigation on Steady Blowing Flow Control within a Compact Inlet Duct," *International Journal of Heat and Fluid Flow*, Vol. 54, 2015, pp. 143–152.

[59] Sahni, O., Zhou, M., Shephard, M. S., and Jansen, K. E., "Scalable implicit finite element solver for massively parallel processing with demonstration to 160K cores," *Proceedings of the Conference on High Performance Computing Networking, Storage and Analysis*, 2009, pp. 68:1–68:12. https://doi.org/http://doi.acm.org/10.1145/1654059.1654129, URL http://doi.acm.org/10.1145/1654059.1654129.

[60] Haller, G., "Distinguished material surfaces and coherent structures in three-dimensional fluid flows," *Physica D*, Vol. 149, 2001, pp. 248–277.

[61] Benettin, G., Galgani, L., Giorgilli, A., and Strelcyn, J., "Lyapunov Characteristic Exponents for Smooth Dynamical Systems and for Hamiltonian Systems; A Method for Computing All of Them. Part 1: Theory," *Meccanica*, Vol. 15, No. 1, 1980, pp. 9–20.

[62] Shadden, S. C., Lekien, F., and Marsden, J. E., "Definition and properties of Lagrangian coherent structures from finite-time Lyapunov exponents in two-dimensional aperiodic flows," *Physica D: Nonlinear Phenomena*, Vol. 212, No. 3-4, 2005, pp. 271–304.

[63] Haller, G., and Yuan, G., "Lagrangian coherent structures and the rate of strain in a partition of two-dimensional turbulence," *Physics of Fluids*, Vol. 12, No. 5, 2000, pp. 1251–1263.

[64] Aurell, E., Boffetta, G., Crisanti, A., Paladin, G., and Vulpiani, A., "Predictability of fluid motions," *Journal of Physics A: Mathematical and General*, Vol. 30, No. 1, 1997, p. 1.

[65] Boffetta, G., Cencini, M., Falcioni, M., and Vulpiani, A., "Detection of a strange attractor in turbulent laboratory convection," *Physical Review E*, Vol. 66, No. 6, 2001.

[66] Lagares, C., and Araya, G., "A GPU-Accelerated Particle Advection Methodology for 3D Lagrangian Coherent Structures in High-Speed Turbulent Boundary Layers," *Energies*, Vol. 16, No. 12, 2023. https://doi.org/10.3390/en16124800, URL https://www.mdpi.com/1996-1073/16/12/4800.

[67] Wu, X., and Moin, P., "A direct numerical simulation study on the mean velocity characteristics in turbulent pipe flow," *Journal of Fluid Mechanics*, Vol. 608, 2008.

[68] P. Schlatter and R. Orlu, "Assessment of direct numerical simulation data of turbulent boundary layers," *Journal of Fluid Mechanics*, Vol. 659, 2010, pp. 116–126.

[69] Skote, M., "Studies of turbulent boundary layer flow through direct numerical simulation," *Royal Institute of Technology, Stockholm, Sweden*, Vol. PhD thesis, 2001.

[70] Kong, H., Choi, H., and Lee, J., "Direct numerical simulation of turbulent thermal boundary layers," *Physics of Fluids*, Vol. 12, No. 10, 2000, pp. 2555–2568.

[71] Spalart, P., "Direct simulation of a turbulent boundary layer up to $Re_\theta = 1410$," *Journal of Fluid Mechanics*, Vol. 187, 1988, pp. 61–98.

[72] Lagares, C., and Araya, G., "Power spectrum analysis in supersonic/hypersonic turbulent boundary layers," *AIAA SCITECH 2022 Forum*, 2022. https://doi.org/10.2514/6.2022-0479, URL https://arc.aiaa.org/doi/abs/10.2514/6.2022-0479.

[73] Osterlund, J.M., "Experimental studies of zero pressure-gradient turbulent boundary-layer flow," Ph.D. thesis, Royal Institute of Technology, Stockholm, Sweden, 2000.

[74] White, F., *Viscous flow*, McGraw Hill, New York, 1974.

[75] Antonia, R., and Chambers, A., "Intermittency in the region of the turbulent boundary layer," *Journal of Fluid Mechanics*, Vol. 55, No. 3, 1972, pp. 459–472.

[76] Adrian, R. J., and Liu, Z., "Observation of vortex packets in Direct Numerical Simulation of fully turbulent channel flow," *Journal of Visualization*, Vol. 5, 2002, pp. 9–19.